

Improvements and gaps in the empirical expressions for the fill factor of modern industrial solar cells



Gaia M.N. Javier^{*}, Priya Dwivedi, Yoann Buratti, Ivan Perez-Wurfl, Thorsten Trupke, Ziv Hameiri

School of Photovoltaic and Renewable Energy Engineering, The University of New South Wales, Sydney, Australia

ARTICLE INFO

Keywords:
Fill factor
Empirical expressions
Ideality factor
Recombination
Non-uniformity

ABSTRACT

This study assesses and improves the accuracy of commonly used expressions for the fill factor (FF). Parameters that could affect the accuracy of the revised expressions are investigated. Empirical coefficients of the commonly used analytical expressions are first recalculated using a modified fitting approach. Although the predictions of the revised expressions perfectly match the results of theoretical one-diode model simulations, gaps are observed when compared with actual measurements. The different impacts of unaccounted factors in the expressions are then explored. It is shown that adjusting the ideality factor or considering edge recombination improves the accuracy of the predictions. Moreover, the expressions can slightly overestimate the FF of cells with non-uniform implied open-circuit voltage distribution. As methods to extract electrical parameters from luminescence images continuously improve, the findings of this study can aid in developing techniques for extracting FF from luminescence images of industrial solar cells.

1. Introduction

The fill factor (FF) is one of the key electrical parameters quantifying the performance of solar cells [1]. The FF is directly proportional to the power conversion efficiency of a solar cell (higher FF leads to higher efficiency). It can be computed from the ratio of the maximum power to the product of the short circuit current I_{sc} and the open circuit voltage V_{oc} . One of the ways to extract these parameters is through the use of the one-diode model [2] equation given as:

$$J = J_L - J_0 \left[\exp\left(\frac{V + JR_s}{nV_T}\right) - 1 \right] - \left(\frac{V + JR_s}{R_{sh}} \right), \quad (1)$$

where J is the current density, J_L is the light generated current density, J_0 is the dark saturation current density, V is the voltage, R_s is the series resistance, n is the ideality factor, V_T is the thermal voltage, and R_{sh} is the shunt resistance.

From Eq 1, Green [3–5] developed explicit expressions for the FF as a function of the normalised values of V_{oc} , R_s , and R_{sh} . The normalised variables are summarised in Table 1 while the explicit expressions for the FF are presented in Table 2.

The explicit expressions contain empirical coefficients C_1 , C_2 , C_3 , C_4 , C_5 that were originally determined by Green via fitting simulated data.

However, the coefficients were only fitted at the extremities of his defined electrical parameter range due to computational limitations at the time of publication (the 1980s) [6]. Also, Green's fitting range represents the electronic properties of common solar cells at that time and is much wider than the electrical parameter range of modern industrial silicon solar cells.

Factors other than the fitting approach and range could impact the accuracy of the expressions [7]: (1) the ideality factor (n) is often assumed to be unity in the one-diode model, however, modern industrial cells typically have $n > 1$ [8,9]; (2) the developed expressions are based on the one-diode model (bulk and surface recombination) [10], however, a two-diode model that considers edge recombination (through a second diode with an ideality factor and dark saturation current density of n_2 and J_{02} respectively [11]) is often found to be more accurate [12–14]; and (3) the one-diode model and two-diode model consider only average values throughout the cells, thus, they may misrepresent non-uniform cells [15,16].

The main objectives of this study are, therefore, to (1) evaluate and improve the accuracy of the explicit expressions for the FF of modern industrial solar cells, and (2) assess the impact of unaccounted factors on the accuracy of the improved expressions.

* Corresponding author.

E-mail address: g.javier@unsw.edu.au (G.M.N. Javier).

Table 1
Normalised electrical parameters [5].

Variable	Description	Formula
v_{oc}	Normalised V_{oc}	V_{oc}/nV_T
R_{ch}	Characteristic resistance	V_{oc}/I_{sc}
r_s	Normalised R_s	R_s/R_{ch}
r_{sh}	Normalised R_{sh}	R_{sh}/R_{ch}

Table 2
Fill factor empirical expressions [5].

Resistance	r_{sh}	
	∞	Finite
r_s	0	$FF_0 = \frac{v_{oc} - \ln(v_{oc} + C_1)}{v_{oc} + 1}$
	Finite	$FF_{sh} = FF_0[1 - \frac{v_{oc} + C_4}{v_{oc}} (\frac{FF_0}{r_{sh}})]$
		$FF_s = FF_0(1 - C_2 r_s) + \frac{r_s^2}{C_3}$
		$FF_{pred} = FF_s[1 - \frac{v_{oc} + \widehat{C}_4}{v_{oc}} (\frac{FF_s}{r_{sh}})]$

2. Methodology

2.1. Recalculation and evaluation of empirical coefficients

A total of 750,000 current-voltage (I-V) curves were simulated based on the one-diode model. Three approaches (namely: A, B, and C) were implemented to determine the empirical coefficients. Approach A replicates Green's approach [6] which fits the coefficients at the limits of his electrical parameter range. Approach B extends Green's approach by fitting the coefficients across his entire range, while Approach C computes the coefficients based on the narrower range of electrical parameters of modern solar cells. In all cases, the empirical coefficients were calculated using the non-linear least-squares method [17] and their accuracy was evaluated through the root mean square error (RMSE) given as [18]:

$$RMSE = \sqrt{\frac{1}{N} \sum (FF_{pred} - FF_{act})^2}, \quad (2)$$

where FF_{pred} is the predicted FF using the explicit expressions, FF_{act} is the simulated/measured value, and N is the total number of data points. The RMSE is related to the mean of the squared errors, thus, highly accurate fits are associated with an RMSE close to zero.

The accuracy of the expressions is evaluated using the simulated curves (750,000) and actual I-V measurements of 15,000 passivated emitter and rear contact (PERC) solar cells [19] from a modern industrial solar cell manufacturing line (with an average efficiency of 23%). Note that a unity ideality factor is initially assumed for the experimental

data; this assumption will be reassessed in the succeeding section. A summary of the procedure is presented in Fig. 1.

2.2. Investigation of unaccounted factors in the explicit expressions

Unaccounted factors in the empirical model, as mentioned in Section 1, are investigated using actual I-V measurements and electroluminescence [20] (EL) images.

The impacts of the ideality factor (n) and of edge recombination (which is attributed to J_{02} [21]) are considered individually. The general framework is illustrated in Fig. 2. The ideality factor of 15,000 industrial solar cells is computed by fitting the V_{oc} , I_{sc} , R_s , and R_{sh} measurements of 1000 randomly selected cells with their measured FF using the non-linear least-squares method. Note that only a subset of the data was used as this is more practical when it comes to the actual application of the fitting in production lines. The individual values are recorded, and the median ideality factor (referred to as the 'effective' ideality factor hereafter) is then applied to the developed empirical expressions. The FF of the entire set of cells is then recalculated and evaluated against the measured FF through the RMSE. The same approach is also implemented to account for edge recombination. The J_{02} of 1000 randomly selected cells is fitted based on the two-diode model. For this study, we assume that the ideality factors of the first and second diode are 1 and 2, respectively. With the addition of the second diode, the expression for the FF becomes more complicated. Thus, the Brent's method [22] is used to solve the two-diode expression.

The impact of a non-uniform distribution of implied open-circuit voltage (iV_{oc}) across the cell is investigated using the solar cell simulation software Griddler 2.5 Pro [23]. Aside from the actual I-V measurements of the 15,000 PERC cells, EL images of the same cells were also provided. These images were used to generate non-uniformity patterns in the Griddler simulations. A "base" image was first created by averaging the EL images of the 100 most uniform cells in the dataset. Ratio images were then generated by dividing each EL image by the base image. Through these ratio images, non-uniformity due to the busbars and fingers was minimised. The degree of non-uniformity is determined by the coefficient of variation (CV) [24]:

$$CV = \frac{\sigma}{\mu}, \quad (3)$$

where σ is the standard deviation and μ is the mean of the pixels. Note that the relationship between the ratio of the luminescence intensities (L_1/L_2) to the implied voltage difference (ΔiV) is as follows:

$$\Delta iV \approx V_T \ln\left(\frac{L_1}{L_2}\right) \quad (4)$$

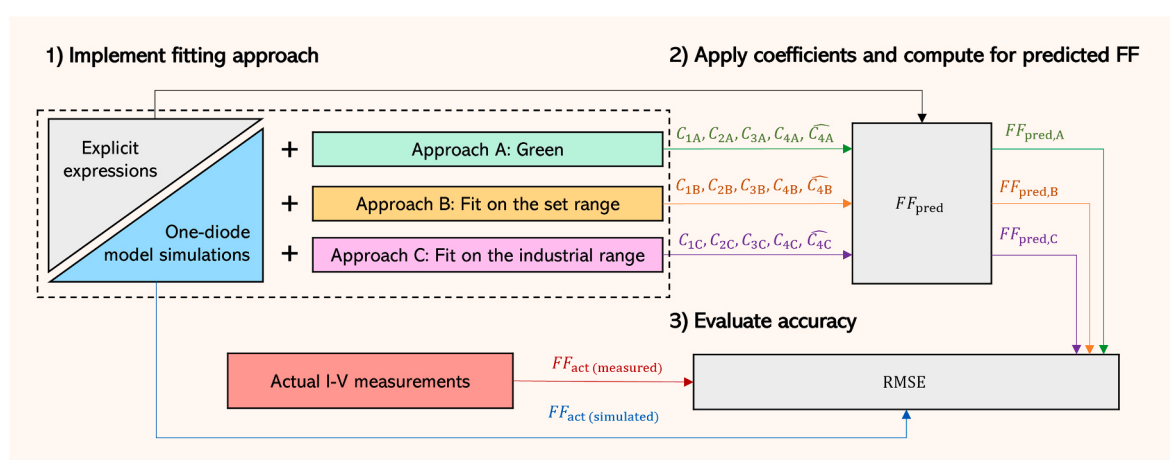


Fig. 1. Methodology for the recalculating and evaluation of the empirical coefficients.

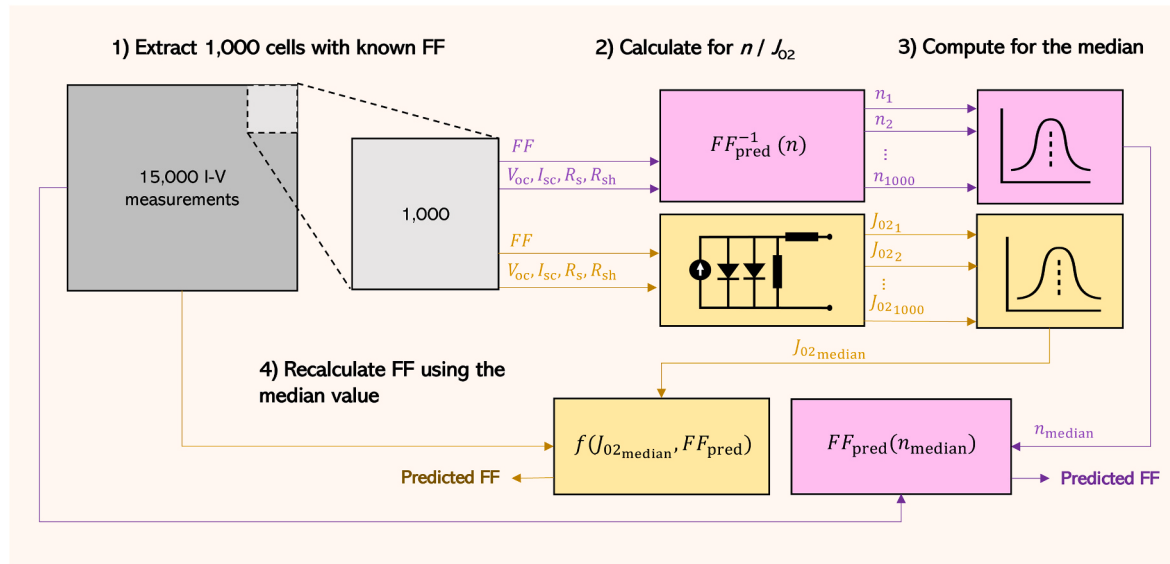


Fig. 2. Methodology for the investigation of ideality factor and edge recombination through the actual I-V measurements.

Given Eq 4, the average iV_{oc} of all the ratio patterns was set to 680 mV, similar to the average V_{oc} of the experimental dataset. The equivalent saturation current density of the first diode (J_{01}) distribution was then computed (to ensure an average iV_{oc} of 680 mV) and applied to Griddler. Typical values for state-of-the-art solar cells were used for the other electrical parameters (see Table A.2). The FF of each of the cells was then determined and compared to the FF of a uniform cell. Fig. 3 illustrates a sample implementation of the methodology on a solar cell with 3×3 pixels. The actual EL images used have 520×520 pixels.

3. Results and discussion

3.1. Recalculation and evaluation of the empirical coefficients

Green's limits are $v_{oc} > 10$, $r_s < 0.4$, and $r_{sh} > 2.5$ (used in Approaches A and B). Assuming $n = 1$, $V_T = 25.69$ mV (at 25°C), and a short-circuit current density $J_{sc} = 40$ mA/cm 2 , then Green's limits are equivalent to $V_{oc} > 257$ mV, $R_s < 7$ $\Omega\cdot\text{cm}^2$, and $R_{sh} > 0.05$ k $\Omega\cdot\text{cm}^2$. With the development of PV technology, modern solar cells have higher V_{oc} and R_{sh} , and lower R_s compared to cells fabricated in the 1980s. In this study, reduced ranges are considered $v_{oc} > 25$, $r_s < 0.08$, and $r_{sh} > 14$ (used in Approach C). With the same assumptions, this is equivalent to $V_{oc} > 642$ mV, $R_s < 1.4$ $\Omega\cdot\text{cm}^2$, and $R_{sh} > 0.24$ k $\Omega\cdot\text{cm}^2$. It can be safely assumed that all current industrial PERC are included in these modified ranges.

A summary of the extracted empirical coefficients from each

approach described above is presented in Table 3. Regardless of the fitting approach and fitting range, the same value for C_2 is derived. However, variations in C_1 , C_3 , and C_4 are observed compared to the original coefficients. \hat{C}_4 was calculated to be zero for all approaches, reducing the expression for FF_{pred} to:

$$FF_{\text{pred}} = FF_s [1 - \left(\frac{FF_s}{r_{sh}}\right)] \quad (5)$$

These coefficients can be adjusted depending on the ideality factor (see Table A.3). Our proposed fitting approach can also be adapted to other cell technologies with a different electrical parameter range.

Fig. 4 shows the errors between the predicted FF (calculated via the different approaches described above) and simulated FF across various ranges of normalised parameters (v_{oc} , r_s , and $1/r_{sh}$). Errors from using Green's coefficients fitted at the extremities ('original') are presented in

Table 3
Fill factor empirical coefficients.

Variables	Green's range		Industrial range
	Approach A ('original')	Approach B	Approach C ('modified')
C_1	0.72	0.72	0.79
C_2	1.1	1.1	1.1
C_3	5.4	6.3	4.0
C_4	0.7	0.8	1.1
\hat{C}_4	0 (but 0.7 in Ref [5])	0	0

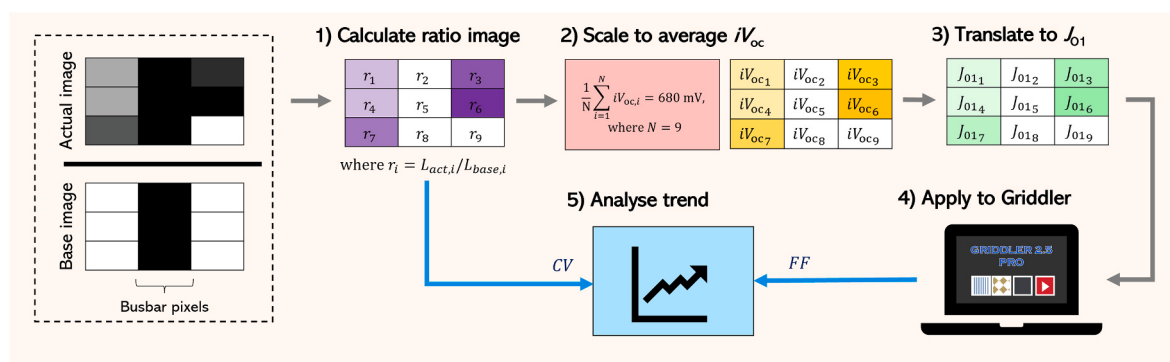


Fig. 3. Methodology for the investigation of non-uniform iV_{oc} through actual EL images. See text for further details.

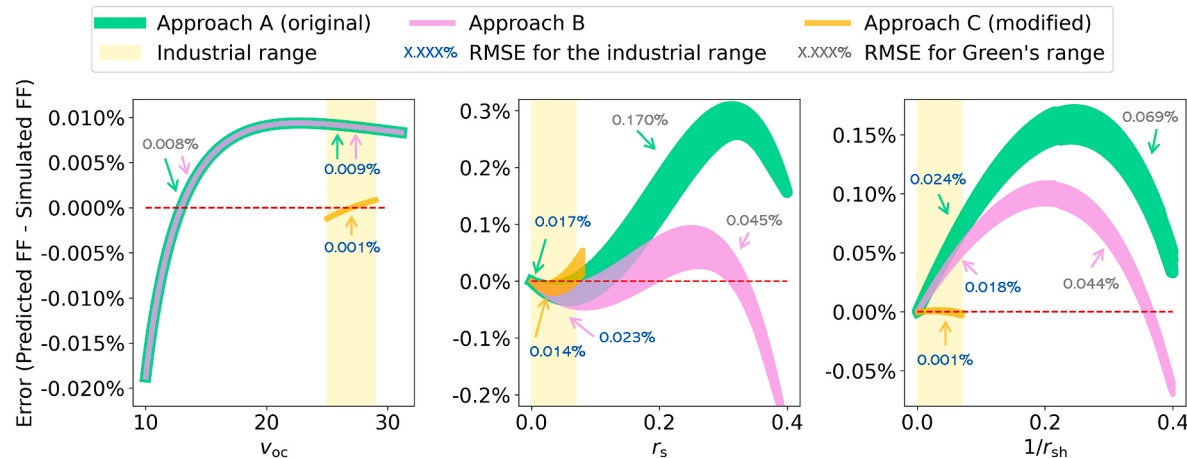


Fig. 4. Error in predicted FF vs normalised electrical parameters.

green (Approach A). As discussed above, in Approach B, the empirical coefficients are fitted across the entire parameter range. Errors due to these coefficients are presented in pink. Lastly, the set of coefficients that is computed by fitting parameters only within the modern industrial range ('modified') is presented in orange (Approach C). The corresponding RMSEs for the industrial range (highlighted in yellow) are also listed.

Generally, it can be observed that the magnitude of errors for r_s and $1/r_{sh}$ is larger compared to that of V_{oc} . This means that the empirical expressions have better accuracy when R_s is negligible and R_{sh} is infinite. Despite using a relatively lower number of simulated samples and fitting only in the extremities of the electrical parameter range (due to computational limitations), the errors associated with the original coefficients are relatively small (with RMSEs of 0.008%, 0.170%, and 0.069% for V_{oc} , r_s , and $1/r_{sh}$, respectively). By expanding the approach to fit the entire range, the coefficients are only slightly changed, resulting in marginal changes in the overall errors (except for r_s which improved the RMSE from 0.170% to 0.045%). By limiting the approach to the industrial range, the errors associated with the expressions are significantly reduced, indicating that the modified coefficients better fit current industrial cells. For r_s , the improved accuracy is less significant in the industrial range, probably because the r_s has a very small value in this range. Hence, the value of C_3 has a small impact on the prediction of FF.

For better visualisation, the accuracy of the modified and original expressions in the typical industrial range of FF for the 750,000

simulated curves is presented in Fig. 5(a). In this range, the modified and original expressions have RMSEs of 0.037% and 0.058%, respectively. Fig. 5(a) shows the cumulative error in FF prediction, whereas Fig. 4 shows the individual errors of each electrical parameter. Thus, errors in Fig. 5(a) are relatively larger than those in Fig. 4.

The accuracy of the expressions evaluated using actual I-V measurements is shown in Fig. 5(b). In this case, the measured I-V parameters (V_{oc} , I_{sc} , R_s , R_{sh}), as reported by an I-V tester, were applied to the empirical expressions to predict the FF. The measured FF of these cells ranges from 79% to 83% (note the indication for density), with the majority of cells exhibiting FF values between 82 and 83%. Although the modified expressions slightly improve the prediction accuracy (RMSE of 0.632% compared to 0.639%), the predictions by both the modified and original expressions fall above the ideal trend, overestimating the FF in all cases. These errors suggest that unaccounted factors in the empirical expressions have a significant impact on the accuracy of these expressions.

3.2. Investigation of unaccounted factors in the empirical expressions

The results above indicate that there are gaps between FF predictions using the analytical expressions and the measured FF. These gaps can be attributed to unaccounted factors in the empirical expressions like a non-unity ideality factor, edge recombination, and cell non-uniformity.

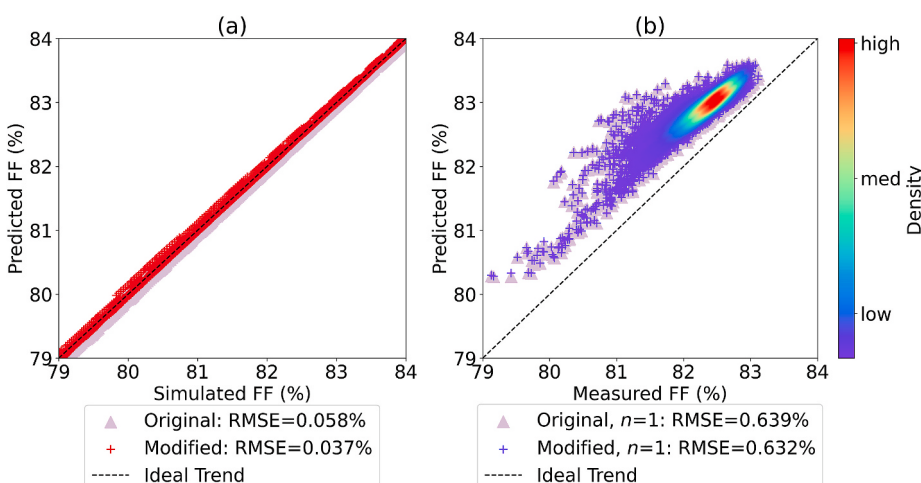


Fig. 5. Predicted FF vs simulated FF (a) and predicted FF vs measured FF (b).

3.2.1. Non-unity ideality factor

The inset of Fig. 6(a) presents the calculated effective ideality factor of 1000 randomly selected cells based on non-linear fitting of the I-V parameters. Most of the cells have an estimated ideality factor of 1.05 ± 0.01 . Note that this value varies between sets of cells, however it can easily be determined for any specific data set.

The effective ideality factor ($n = 1.05$) for the 1000 cells is then applied to the whole dataset. The predicted FF as a function of the measured FF is shown in Fig. 6(a). As can be seen, the prediction remarkably improves with most of the predictions already coinciding with the actual measurements and the RMSE reduces from 0.632% to 0.161%. Hence, the empirical predictions can be significantly improved if a subset of the data is used to determine an effective ideality factor and is applied to the whole dataset.

3.2.2. Edge recombination

The J_{02} distribution of 1000 randomly selected cells is shown in the inset of Fig. 6(b). Note that J_{02} is implicit in the two-diode model, but it can be extracted through numerical methods. Here, the Brent's method [22] was used. For most cells, J_{02} is within the range of $3 \pm 1 \text{ nA/cm}^2$.

Fig. 6(b) presents the predicted FF as a function of the measured FF after applying the effective J_{02} to the two-diode model. Similar to the impact of the ideality factor (Section 3.2.1), the prediction accuracy improves when J_{02} is considered (RMSE reduces from 0.632% to 0.164%). Hence, considering the edge recombination significantly increases the accuracy of estimating FF.

Though not visible in the graphs, adding a non-unity ideality factor and edge recombination have slightly different impacts. Note that the non-unity ideality factor considers the one-diode model while the edge recombination considers the two-diode model to represent the solar cells (hence, both bulk and edge recombination are considered).

3.2.3. Non-uniformity

Previous sections show that having more parameters (n or J_{02}) may allow fitting cell I-V data of cells more accurately. In this section, the impact of accounting for spatially dependent parameters is explored. A set of 250 randomly selected EL images of cells with $<0.1\%$ error in the predicted FF (referred to below as ‘correctly estimated’ cells) and another set of 250 randomly selected EL images of cells with $>0.5\%$ error (‘highly overestimated’ cells) were studied in Griddler 2.5 Pro. Fig. 7(a–c) presents sample iV_{oc} maps of a uniform ‘base’ cell, a correctly estimated cell, and a highly overestimated cell. In the uniform case, the iV_{oc} is 680 mV throughout the cell, thus $CV = 0$. For the correctly

estimated cell, $CV = 0.22\%$ where the iV_{oc} ranges from 670 to 690 mV. For the highly overestimated cell, several regions fall below 670 mV resulting in a higher CV (0.54%).

Fig. 8(a) illustrates the CV distribution of the investigated cells. Results show that the highly overestimated cells are less uniform with an average CV of 0.42% compared to those lying on the ideal trend that have an average CV of 0.25%. Fig. 8(b) shows the FF error distribution between the uniform and non-uniform cells. The average errors for the correctly estimated and highly overestimated cells are -0.01% and -0.03% , respectively. Hence, having a non-uniform iV_{oc} can result in a slightly overestimated FF. Furthermore, as the non-uniformity increases, the degree of overestimation increases. Additional simulations show that if the non-uniformity is equivalent to $CV = 1.5\%$ (equivalent to a standard deviation of $\sim 10 \text{ mV}$ for an average iV_{oc} of 680 mV), then the overestimation in FF would be around 0.2% (absolute). It was also observed that the effect of non-uniform iV_{oc} on the FF prediction decreases as R_s becomes negligible (as without resistance, the carriers tend to uniformly distribute across the cell).

3.2.4. Additional investigation

Uncertainties in the input parameters (the measured I-V parameters) can also impact the accuracy of the FF predictions. As we did not have access to the I-V tester or to the measured cells during this study (the data was provided by an industry partner), we investigated the distributions of the key electrical parameters. Solar cells with $>0.5\%$ absolute error in the predicted FF (Fig. 6) were identified and analysed. Fig. 9 compares the R_{sh} and V_{oc} distributions of the overestimated cells (in green) and the whole population (in pink). The R_{sh} values for the cells with large errors in the predicted FF (green histograms) are heavily skewed towards lower shunt resistance values, with a large fraction of cells exhibiting shunt values $< 200 \text{ k}\Omega\cdot\text{cm}^2$. Those same cells exhibit only a minor reduction in V_{oc} (with a median of $\approx 677 \text{ mV}$, compared to 680 mV for the whole set). Based on simulations [25], the V_{oc} of cells with such a low R_{sh} should be below 600 mV. Therefore, the overestimation of some of the investigated cells can also be due to errors in I-V measurements, however, this is outside the scope of this study and requires further investigation. As previous studies have shown the capability of luminescence images to capture pertinent parameters like iV_{oc} [26], R_s [27], and R_{sh} [28], future work may focus on directly extracting these parameters from luminescence images to solve for FF and eradicate potential errors from I-V measurements.

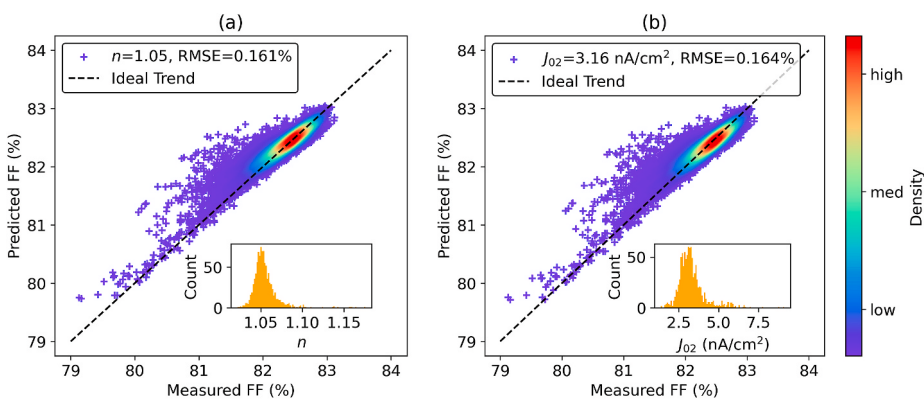


Fig. 6. Impact on FF prediction of (a) non-unity ideality factor and (b) edge recombination. Graphs show the predicted FF vs measured FF after incorporating the effective values. Insets show the computed n - and J_{02} distributions, respectively, of 1000 randomly selected cells.

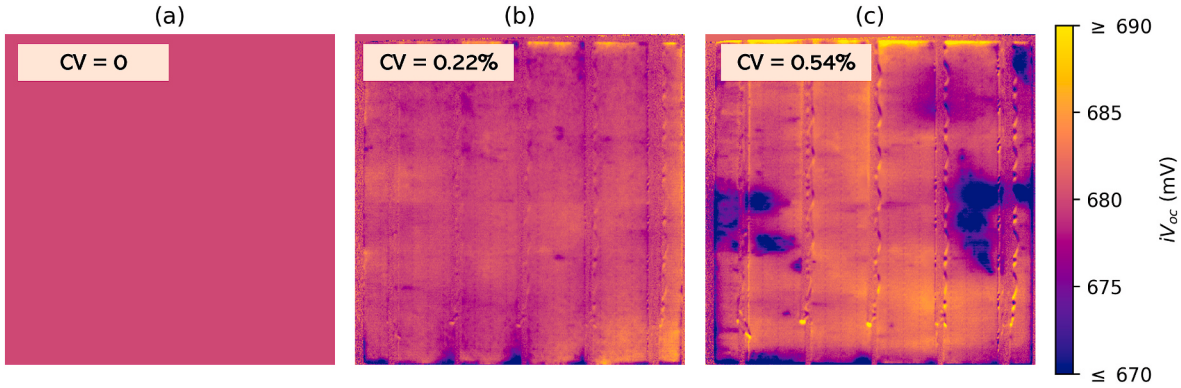


Fig. 7. Example of iV_{oc} maps of (a) a uniform base cell, (b) a correctly estimated cell, (c) a highly overestimated cell.

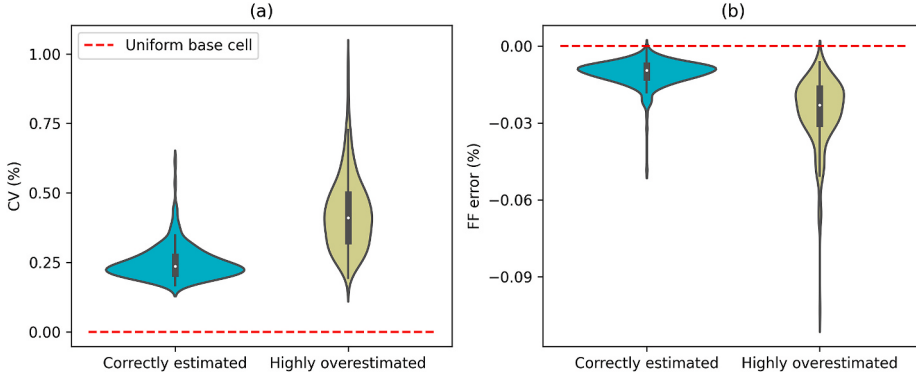


Fig. 8. (a) CV and (b) FF error of 250 correctly estimated cells and 250 highly overestimated cells compared to a uniform 'base' cell.

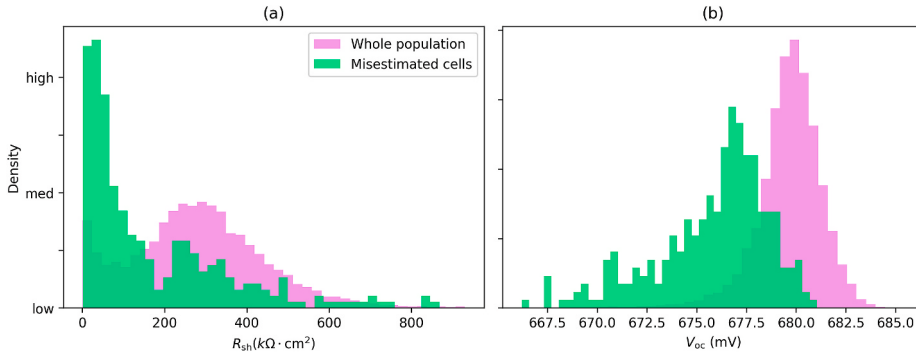


Fig. 9. (a) R_{sh} and (b) V_{oc} distribution of overestimated cells vs the whole population.

4. Conclusion

The accuracy of previously published FF expressions was evaluated and improved for modern industrial silicon solar cells. A revised approach that fits the empirical coefficients to the industrial solar cell electrical parameter range is proposed. The revised coefficients improve

the accuracy of the expressions and match the one-diode model simulations. However, when the analytical expressions for the FF were applied to a large set of experimental I-V data obtained from industrial solar cells, relatively large errors between predicted and measured FF were observed. Unaccounted factors in the empirical expressions were then investigated. It was shown that if the ideality factor (n) or edge

recombination (J_{02}) is known, the accuracy of the predictions significantly increases. It was also demonstrated that non-uniform cell parameters such as the iV_{oc} can result in a slight overestimation of the FF. Besides improving the accuracy of commonly used expressions, this study can help develop methods to extract the FF directly from luminescence images as methods to extract R_s , R_{sh} , and iV_{oc} from images evolve and improve.

CRediT authorship contribution statement

Gaia M.N. Javier: Methodology, Investigation, Formal analysis, Conceptualization, Visualization, Writing – original draft, Writing – review & editing. **Priya Dwivedi:** Methodology, Writing – review & editing. **Yoann Buratti:** Methodology, Writing – review & editing. **Ivan Perez-Wurfl:** Methodology, Writing – review & editing. **Thorsten Trupke:** Methodology, Formal analysis, Writing – review & editing. **Ziv Hameiri:** Supervision, Methodology, Conceptualization, Formal analysis, Investigation, Writing – review & editing.

Appendix

A.1. Derivation of FF_0 expression for the one-diode model [29]

The one diode model without the effect of resistance is given by:

$$I = I_L - I_0 \left[\exp\left(\frac{V}{nV_T}\right) - 1 \right]. \quad (\text{A.1})$$

For V_{oc} ($I = 0$) and I_{sc} ($V = 0$) this results in:

$$V_{oc} = nV_T \ln\left(\frac{I_0 + I_L}{I_0}\right), \quad (\text{A.2})$$

$$I_{sc} = I_L. \quad (\text{A.3})$$

Substituting Eq A.2 and A.3 into Eq A.1 gives:

$$I_0 = \frac{I_{sc}}{\exp(V_{oc}/nV_T) - 1}, \quad (\text{A.4})$$

$$I = I_{sc} \left[1 - \frac{\exp(V/nV_T) - 1}{\exp(V_{oc}/nV_T) - 1} \right]. \quad (\text{A.5})$$

Multiply Eq A.5 by V to get the power (P):

$$P = V \cdot I = V \cdot I_{sc} \left[1 - \frac{\exp(V/nV_T) - 1}{\exp(V_{oc}/nV_T) - 1} \right]. \quad (\text{A.6})$$

Differentiate Eq A.6 with respect to V :

$$\frac{dP}{dV} = I_{sc} \left[1 - \left(\frac{V}{nV_T} \frac{\exp(V/nV_T)}{\exp(V_{oc}/nV_T) - 1} - \frac{\exp(V/nV_T) - 1}{\exp(V_{oc}/nV_T) - 1} \right) \right]. \quad (\text{A.7})$$

Solve for the voltage at the maximum power point V_{mp} (V where $dP/dV = 0$):

$$I_{sc} \left[1 - \left(\frac{V_{mp}}{nV_T} \frac{\exp(V_{mp}/nV_T)}{\exp(V_{oc}/nV_T) - 1} - \frac{\exp(V_{mp}/nV_T) - 1}{\exp(V_{oc}/nV_T) - 1} \right) \right] = 0, \quad (\text{A.8})$$

$$V_{mp} = nV_T \left[W\left(\exp(V_{oc}/nV_T) + 1\right) - 1 \right], \quad (\text{A.9})$$

where $W[\exp(V_{oc}/nV_T) + 1]$ is the Lambert function of $[\exp(V_{oc}/nV_T) + 1]$.

An approximation of the Lambert function is given by [for $x \geq e$ (≈ 2.72)]:

$$W(x) = \ln(x) - \ln(\ln(x)). \quad (\text{A.10})$$

Therefore, V_{mp} can be simplified as:

$$V_{mp} = V_{oc} - nV_T \left[\ln\left(\frac{V_{oc}}{nV_T} + 1\right) \right]. \quad (\text{A.11})$$

Declaration of competing interest

The authors declare that they have no known competing financial interests or personal relationships that could have appeared to influence the work reported in this paper.

Data availability

The data from this study are available from the corresponding author, G.M.N. Javier, upon reasonable request.

Acknowledgment

This work was supported by the Australian Government through the Australian Renewable Energy Agency (ARENA, Grant 2020/RND016). The views expressed herein are not necessarily the views of the Australian Government, and the Australian Government does not accept responsibility for any information or advice contained herein.

Solve for the corresponding current I_{mp} :

$$I_{mp} = I_{sc} \left[1 - \frac{\exp(V_{mp}/nV_T) - 1}{\exp(V_{oc}/nV_T) - 1} \right] \quad (\text{A.12})$$

$$I_{mp} = \frac{I_{sc}}{(1 + nV_T/V_{oc})(1 - \exp(-V_{oc}/nV_T))} \quad (\text{A.13})$$

$$I_{mp} = \frac{I_{sc}}{(1 + nV_T/V_{oc})}. \quad (\text{A.14})$$

Solve for FF_0 :

$$FF_0 = \frac{V_{mp}I_{mp}}{V_{oc}I_{sc}} \quad (\text{A.15})$$

$$FF_0 = \frac{V_{oc}/nV_T - \ln(V_{oc}/nV_T + 1)}{(V_{oc}/nV_T + 1)}. \quad (\text{A.16})$$

Defining:

$$v_{oc} = V_{oc} / nV_T \quad (\text{A.17})$$

$$FF_0 = \frac{v_{oc} - \ln(v_{oc} + 1)}{(v_{oc} + 1)} \quad (\text{A.18})$$

Green discovered that modifying the above expression to:

$$FF_0 = \frac{v_{oc} - \ln(v_{oc} + 0.72)}{(v_{oc} + 1)} \quad (\text{A.19})$$

yields more accurate results [5].

A.2. Derivation of the FF_0 expression for the two-diode model

The two-diode model without the effect of resistance is given by Eq A.20.

$$I = I_L - I_{01} \left[\exp \left(\frac{V}{V_T} \right) \right] - I_{02} \left[\exp \left(\frac{V}{2V_T} \right) \right]. \quad (\text{A.20})$$

V_{oc} and I_{sc} can be expressed by:

$$V_{oc} = V_T \ln \left[\frac{I_{02}^2 + 2I_{01}I_L - I_{02}\sqrt{4I_{01}I_L + I_{02}^2}}{2I_{01}^2} \right], \quad (\text{A.21})$$

$$I_{sc} = I_L. \quad (\text{A.22})$$

Express I in terms of V_{oc} and I_{sc} .

$$I = I_{sc} - I_{02} \exp \left(\frac{V}{2V_T} \right) + I_{02} \sqrt{\exp \left(\frac{3V_{oc}}{V_T} \right)} \cdot \exp \left(\frac{V}{V_T} - \frac{2V_{oc}}{V_T} \right) - I_{sc} \exp \left(\frac{V}{V_T} - \frac{V_{oc}}{V_T} \right). \quad (\text{A.23})$$

P is expressed as:

$$P = V \left[I_{sc} - I_{02} \exp \left(\frac{V}{2V_T} \right) + I_{02} \sqrt{\exp \left(\frac{3V_{oc}}{V_T} \right)} \cdot \exp \left(\frac{V}{V_T} - \frac{2V_{oc}}{V_T} \right) - I_{sc} \exp \left(\frac{V}{V_T} - \frac{V_{oc}}{V_T} \right) \right] \quad (\text{A.24})$$

while dP/dV is given by:

$$\frac{dP}{dV} = -\frac{I_{02}V \exp \left(\frac{V}{2V_T} \right)}{2V_T} + \frac{I_{02}V \sqrt{\exp \left(\frac{3V_{oc}}{V_T} \right)} \exp \left(\frac{V}{V_T} - \frac{2V_{oc}}{V_T} \right)}{V_T} - I_{02} \exp \left(\frac{V}{2V_T} \right) + I_{02} \sqrt{\exp \left(\frac{3V_{oc}}{V_T} \right)} \exp \left(\frac{V}{V_T} - \frac{2V_{oc}}{V_T} \right) - \frac{I_{sc}V \exp \left(\frac{V}{V_T} - \frac{V_{oc}}{V_T} \right)}{V_T} - I_{sc} \exp \left(\frac{V}{V_T} - \frac{V_{oc}}{V_T} \right) + I_{sc}. \quad (\text{A.25})$$

V_{mp} cannot be solved explicitly because there are no analytical solutions to $dP/dV = 0$.

A.3. One-diode model simulations

One-diode model simulations were used to recalculate the empirical coefficients of the FF expressions. Table A.1 summarises the range of input parameters to the one-diode model simulations. Various combinations of these parameters were used, and the corresponding FF values were calculated. The empirical coefficients were then calculated through non-linear fitting on the different ranges of the normalised electrical parameters.

Table A.1
One-diode model input parameters.

Parameter	Lower limit	Upper limit
J_L – light-generated current density (mA/cm ²)	37	43
V_{oc} – open-circuit voltage (mV)	250	800
R_s – series resistance ($\Omega \cdot \text{cm}^2$)	0	10
R_{sh} – shunt resistance ($\text{k}\Omega \cdot \text{cm}^2$)	0.05	100
n – ideality factor	1	1.3
V_T – thermal voltage (mV)	25.69	25.69

A.4. Griddler simulations

Griddler simulations were used to evaluate the effect of non-uniform distributions of the iV_{oc} on the estimation of the FF. Table A.2 summarises the input parameters for these simulations. Different non-uniformity patterns (that are representative of the measured cells) were introduced for the front saturation current density (J_{01}), however, the *mean* value was kept constant. The resulting EL images and their corresponding FF values were extracted from the simulations. The non-uniformity of these images was computed and then mapped with respect to the simulated FF.

Table A.2
Griddler input parameters of the front (F) and rear (R) layers.

Parameter	Input
H-pattern design page	
Wafer shape	Square
Ingot diameter (cm)	22.3
Wafer length/width (cm)	15.875
Wafer thickness (um)	175
FR – No. of busbars	5
FR – Probe points	30
F – Busbar width (mm)	1
FR – Print method	Single print
F – No. of fingers	131
R – No. of fingers	158
FR – Finger width (μm)	35
FR – End joining	All
FR – Edge gap (mm)	0.6
Rear pattern	Line contact, full area metal
Simulation page	
Wafer internal resistance	0
Internal shunt conductance	0
F – Finger sheet resistance (mΩ/sq)	2.82
F – Finger contact resistance (mΩ · cm ²)	1
F – Illumination (Sun)	1
F – J_{01} , passivated area (fA/cm ²)	140
F – Layer sheet resistance (Ω/sq)	120
R – Layer sheet resistance (Ω/sq)	61
FR – Current extraction	At each probe point
FR – Contact points resistance	0
FR – 1-Sun J_L , non-shaded (mA/cm ²)	43.9
FR – J_{01} , metal contact	0
R – Finger sheet resistance (mΩ/sq)	11.67
R – Finger contact resistance (mΩ · cm ²)	3
R – Illumination	0
R – J_{01} , passivated area	0

A.5 Empirical coefficients for varying the ideality factor

Table A.3
Empirical coefficients for varying ideality factor (industrial range).

Ideality factor range	C_1	C_2	C_3	C_4	\hat{C}_4
1.00–1.05	0.79	1.1	4.0	1.1	0
1.05–1.10	0.79	1.1	4.8	1.1	0
1.10–1.15	0.78	1.1	5.5	1.1	0
1.15–1.20	0.78	1.1	6.7	1.1	0
1.20–1.25	0.77	1.1	8.3	1.1	0
1.25–1.30	0.77	1.1	10.8	1.1	0

References

- [1] M.A. Green, Accurate expressions for solar cell fill factors including series and shunt resistances, *Appl. Phys. Lett.* 108 (8) (2016), 081111.
- [2] M. Theristis, V. Venizelou, G. Makrides, G.E. Georgiou, Chapter II-1-B - Energy yield in photovoltaic systems, in: McEvoy's Handbook of Photovoltaics, third ed., Academic Press, 2018, pp. 671–713.
- [3] M.A. Green, General solar cell curve factors including the effects of ideality factor, temperature and series resistance, *Solid State Electron.* 20 (3) (1977) 265–266.
- [4] M.A. Green, Solar cell fill factors: general graph and empirical expressions, *Solid State Electron.* 24 (8) (1981) 788–789.
- [5] M.A. Green, Accuracy of analytical expressions for solar cell fill factors, *Sol. Cell.* 7 (3) (1982) 337–340.
- [6] Private Communication, e-mail, 2021.
- [7] G.M. Javier, P. Dwivedi, Y. Buratti, T. Trupke, Z. Hameiri, Fill factor prediction of modern industrial cells: Potential gaps and improvements, in: presented at the 49th IEEE Photovoltaic Specialists Conference, 2022.
- [8] M. Leilaeioun, Z.C. Holman, Accuracy of expressions for the fill factor of a solar cell in terms of open-circuit voltage and ideality factor, *J. Appl. Phys.* 120 (12) (2016), 123111.
- [9] M. Bashahu, P. Nkundabakura, Review and tests of methods for the determination of the solar cell junction ideality factors, *Sol. Energy* 81 (7) (2007) 856–863.
- [10] F. Ghani, G. Rosengarten, M. Duke, J.K. Carson, The numerical calculation of single-diode solar-cell modelling parameters, *Renew. Energy* 72 (2014) 105–112.
- [11] K. McIntosh, C. Honsberg, The influence of edge recombination on a solar cell's IV curve, in: presented at the 16th European Photovoltaic Solar Energy Conference, 2000.
- [12] A.M. Humada, M. Hojabri, S. Mekhilef, H.M. Hamada, Solar cell parameters extraction based on single and double-diode models: a review, *Renew. Sustain. Energy Rev.* 56 (2016) 494–509.
- [13] K.H. Min, et al., An analysis of fill factor loss depending on the temperature for the industrial silicon solar cells, *Energies* 13 (11) (2020) 2931.
- [14] A. Khanna, T. Mueller, R.A. Stangl, B. Hoex, P.K. Basu, A.G. Aberle, A fill factor loss analysis method for silicon wafer solar cells, *IEEE J. Photovoltaics* 3 (4) (2013) 1170–1177.
- [15] H. Haug, M.S. Wiig, R. Søndenå, J. Wong, Simulating the effect of lifetime non-uniformity on solar cell performance using cmd-PC1D 6 and Griddler 2, *Energy Proc.* 92 (2016) 69–74.
- [16] S. Tahir, A. Ali, N. Amin, M.I. Arshad, The effect of nonuniform emitter sheet resistance on PERC solar cell performance, *Silicon* 11 (1) (2019) 393–399.
- [17] M.R. Osborne, Nonlinear least squares — the Levenberg algorithm revisited, *ANZIAM J.* 19 (3) (1976) 343–357.
- [18] C.F.M. Coimbra, J. Kleissl, R. Marquez, Overview of solar-forecasting methods and a metric for accuracy evaluation, in: *Solar Energy Forecasting and Resource Assessment*, Elsevier, 2013, pp. 171–194.
- [19] M.A. Green, The passivated emitter and rear cell (PERC): from conception to mass production, *Sol. Energy Mater. Sol. Cells* 143 (2015) 190–197.
- [20] T. Fuyuki, H. Kondo, T. Yamazaki, Y. Takahashi, Y. Uraoka, Photographic surveying of minority carrier diffusion length in polycrystalline silicon solar cells by electroluminescence, *Appl. Phys. Lett.* 86 (26) (2005), 262108.
- [21] A. Fell, J. Schön, M. Müller, N. Wöhrl, M.C. Schubert, S.W. Glunz, Modeling edge recombination in silicon solar cells, *IEEE J. Photovoltaics* 8 (2) (2018) 428–434.
- [22] R.P. Brent, *Algorithms for Minimization without Derivatives*, Courier Corporation, 2013.
- [23] J. Wong, Griddler: intelligent computer aided design of complex solar cell metallization patterns, in: presented at the 39th IEEE Photovoltaic Specialists Conference, 2013.
- [24] N.L. Johnson, F.C. Leone, Statistics and experimental design, in: *Engineering and the Physical Sciences*, Wiley, New York, NY, 1964.
- [25] P.V. Lighthouse, Dec. 26, 2021, <https://www.pvlighthouse.com.au/equivalent-t-circuit>.
- [26] B. Hallam, B. Tjahjono, T. Trupke, S. Wenham, Photoluminescence imaging for determining the spatially resolved implied open circuit voltage of silicon solar cells, *J. Appl. Phys.* 115 (4) (2014), 044901.
- [27] T. Trupke, E. Pink, R.A. Bardos, M.D. Abbott, Spatially resolved series resistance of silicon solar cells obtained from luminescence imaging, *Appl. Phys. Lett.* 90 (9) (2007), 093506.
- [28] Y. Augarten, et al., Calculation of quantitative shunt values using photoluminescence imaging, *Prog. Photovoltaics Res. Appl.* 21 (5) (2013) 933–941.
- [29] K. Tarett, M. Soldera, M. Troviano, Accurate explicit equations for the fill factor of real solar cells—applications to thin-film solar cells, *Prog. Photovoltaics Res. Appl.* 21 (7) (2013) 1489–1498.